CALCULATION OF POTENTIAL AND CONCENTRATION GRADIENTS IN TRICKLE-BED ELECTRODES PRODUCING HYDROGEN PEROXIDE

Otomar ŠPALEK

Institute of Inorganic Chemistry,
Czechoslovak Academy of Sciences, 160 00 Prague 6

Received April 18th, 1985

A mathematical model for describing the trickle-bed electrode has been developed and used to calculate the potential distribution along the current flow and the hydrogen peroxide concentration profile along the electrolyte flow (normal to the direction of current). Polarization curves and dependences of the current yield of hydrogen peroxide and the peroxide losses due to the processes occurring (reduction, decomposition, and transport into the anode chamber) on the current density have also been calculated. A comparison is made between calculated and measured dependences of the current yield of hydrogen peroxide on the current density.

The preparation of hydrogen peroxide by the cathodic reduction of oxygen in a trickle-bed electrode has lately been the subject of experimental studies at several laboratories[1-5]. The transition to this type of three-dimensional electrode from the previously studied gas diffusion electrodes was motivated mainly by difficulties encountered in operating large-scale diffusion electrodes.

A trickle-bed electrode consists of a bed of crushed electrode material **1** compressed between a plate current collector **2** and a diaphragm **5** (see Fig. 1). A mixture of an alkaline electrolyte (usually a sodium hydroxide solution) and oxygen or air is passed through the bed in co-current flow. Oxygen dissolves in the electrolyte flowing down over the surface of graphite particles and is reduced to form perhydroxyl ions:

$$O_2 + H_2O + 2e^- \rightarrow HO_2^- + OH^- . \qquad (A)$$

In addition to this reaction, other processes must be taken into consideration, namely the reduction of the perhydroxyl ions at the cathode,

$$HO_2^- + H_2O + 2e^- \rightarrow 3\,OH^- , \qquad (B)$$

the chemical decomposition of the peroxide,

$$HO_2^- \rightarrow OH^- + 1/2\,O_2 , \qquad (C)$$

and the transport of perhydroxyl ions into the anode chamber where they are oxidized at the anode.

The electrolyte is fed into each electrode chamber separately, or into the anode chamber from which it flows across the diaphragm into the cathode chamber. In the simplest arrangement, the cathode chamber is operated in a flow mode and the electrolyte gets into the anode chamber only by transport across the diaphragm, while oxygen formed at the anode passes through the diaphragm in the opposite direction.

The study of the processes occurring in a trickle-bed electrode is considerably complicated by a large number of input parameters which affect the potential and concentration gradients within the electrode. Among these are primarily the electrode material, which determines the rates of the reactions occurring, the wettability of the material, the particle size, the macro- and microporosity of the electrode, the gas and electrolyte flow rates, the physical properties of the diaphragm, the pressure in the system, and the current flowing through the cell. Potential measurements on trickle-bed electrodes have been reported in the literature[4,5] and also made in our laboratory. Owing to appreciable local inhomogeneities of the flow, however, the measured potentials are not quite reliable.

The first attempt to describe mathematically the performance of the trickle-bed electrode was made by Oloman and Watkinson[2]. To calculate the rate of oxygen transport in the electrode, they used relations obtained from measurements on non-electrochemical trickle-bed reactors. The applicability of these relations is, however, questionable, since they apply to trickle-beds packed with particles of size at least an order of magnitude larger than that of trickle-bed electrodes. A fairly general formulation of equations for the distributions of the potential and of ion concentrations has been presented by Levin and Oloman[6]. However, despite a number of approximations (*e.g.*, the neglecting of transport limitations and the chemical decomposition of peroxide within the electrode), the proposed mathematical description was so complex that the authors did not attempt to obtain a solution.

The aim of the present work was to calculate the concentration and potential gradients within a trickle-bed electrode, taking into account the transport and kinetic limitations, and to compare the calculated and measured results.

CALCULATION PROCEDURE

The mass transfer coefficient for oxygen transport from the gas phase to the surface of the electrode material was calculated on the basis of flow parameters. This value,

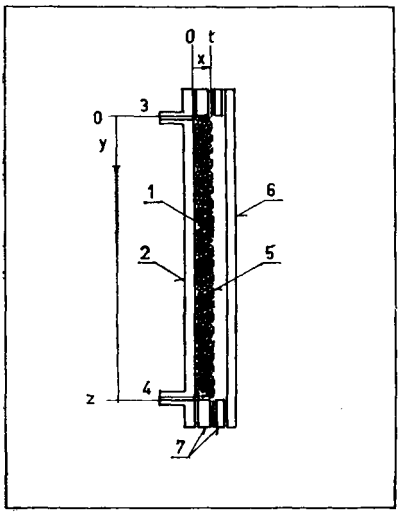

FIG. 1

Trickle-bed electrochemical cell. **1** crushed electrode material; **2** current collector; **3** entry of gas and electrolyte; **4** exit of gas and electrolyte; **5** diaphragm; **6** anode; **7** sealing

together with kinetic constants of oxygen reduction, was used to calculate the potential distribution through the electrode in the direction of the current. The knowledge of the potential profile was used to express the local reaction rates appearing in the differential equation for the distribution of the peroxide concentration in the direction of the electrolyte flow. Integration of this equation yielded the distribution of the peroxide concentration along the electrode height. Next, the current yield of hydrogen peroxide and the peroxide losses due to the various processes were evaluated. The calculation procedure is described in detail in the following paragraphs.

Calculation of Mass Transfer Coefficients

Single-phase pressure drops in the fixed bed are obtained from the Ergun equations[7]

$$\Delta P_G = \frac{(150 + 1{\cdot}75\ \mathrm{Re}_G)\,\mu_G U_G (1 - \varepsilon)^2}{d'^2 \varepsilon^3} \tag{1}$$

$$\Delta P_L = \frac{(150 + 1{\cdot}75\ \mathrm{Re}_L)\,\mu_L U_L (1 - \varepsilon)^2}{d'^2 \varepsilon^3} . \tag{2}$$

The particle diameter, d', modified to account for the high ratio of particle size to bed thickness can be calculated from the effective particle diameter and the bed dimensions as follows:

$$d' = d \Big/ \left[1 + \frac{(t_e + w)\,d}{3 t_e w (1 - \varepsilon)}\right] . \tag{3}$$

The effective particle diameter, d, is obtained from the average mesh size of the electrode material and the particle roughness factor,

$$d = \bar{d}/f_p . \tag{3a}$$

The Reynolds number for a gas in a porous bed is defined as

$$\mathrm{Re}_G = \frac{d' U_G h_G}{\mu_G (1 - \varepsilon)} , \tag{4}$$

and that for a liquid is defined in an analogous manner. From the single-phase pressure drops, the pressure drop for a two-phase medium[8] is calculated as

$$\Delta P_{LG} = \Delta P_L \left[1{\cdot}30 + 1{\cdot}85 \left(\frac{\Delta P_L}{\Delta P_G}\right)^{-0.425}\right]^2 . \tag{5}$$

The value of the two-phase pressure drop can be used to calculate the modified Galileo number,

$$\mathrm{Ga}_\mathrm{L} = \frac{d'^3 h_\mathrm{L}(h_\mathrm{L} g + \Delta P_\mathrm{LG})}{\mu_\mathrm{L}^2}, \tag{6}$$

and this, in turn, allows the liquid hold-up within the electrode[9] to be calculated from

$$\beta = 3{\cdot}86\ \mathrm{Re}_\mathrm{L}^{0.545}\mathrm{Ga}_\mathrm{L}^{-0.42}\left(\frac{ad'}{\varepsilon}\right)^{0.65}. \tag{7}$$

The gas-side and liquid-side mass transfer coefficients at the g–l interface may be estimated from the empirical correlations of Reiss[10]:

$$K_\mathrm{G}a = 2{\cdot}0 + 0{\cdot}69(\Delta P_\mathrm{LG} U_\mathrm{G})^{0.67} \tag{8}$$

$$K_\mathrm{L}a = 0{\cdot}0173\,(\Delta P_\mathrm{LG} U_\mathrm{L})^{0.5}. \tag{9}$$

The liquid-side mass transfer coefficient at the l–s interface is obtained from the relation of Satterfield[11]

$$K_\mathrm{S}a = \frac{0{\cdot}429}{\beta}\,\mathrm{Re}_\mathrm{L}^{0.5}\mathrm{Sc}_\mathrm{L}^{0.33} a^2 D. \tag{10}$$

The overall gas to solid transfer coefficient is given by the relation

$$K_0 = \left(\frac{1}{K_\mathrm{G}} + \frac{1}{K_\mathrm{L}} + \frac{1}{K_\mathrm{S}}\right)^{-1} \tag{11}$$

based on the simplifying assumption that the g–l and l–s interfacial areas are the same. This is true if the liquid flows down as a film over the surface of the electrode material particles. Apparently, such a picture is reasonable for an inappreciable filling of the pores between the particles with the electrolyte and for a relatively large size of electrode material particles.

Calculation of the Potential Profile in the Direction of the Current

The oxygen flux from the gas to the electrode material surface may be expressed as

$$N = K_0(c_0 - c_\mathrm{s}). \tag{12}$$

The rate of peroxide generation by reaction (*A*) is

$$r_1 = \frac{j_1}{2F} = k_1 c_s \exp\left(-\frac{\alpha_1 FE}{RT}\right). \tag{13}$$

Assuming that all of the reacting oxygen comes from the gas phase (this is true if oxygen formed by the heterogeneous decomposition of hydrogen peroxide can be neglected), we can equate the left-hand sides of Eqs (*12*) and (*13*). After rearrangement we obtain an equation giving the current density of oxygen reduction as a function of the local electrode potential:

$$j_1 = \frac{2Fc_0}{K_0^{-1} + k_1^{-1} \exp\left(\alpha_1 FE/RT\right)}. \tag{14}$$

The local electrode potential is given by

$$E = \varphi_1 - \varphi_2 + \text{constant}. \tag{15}$$

If the voltage drop in the electrode material is negligible, we have

$$E = \text{constant} - \varphi_2. \tag{16}$$

The potential gradient in the electrolyte is obtained from Ohm's law as

$$\frac{\mathrm{d}\varphi_2}{\mathrm{d}x} = -\frac{\mathrm{d}E}{\mathrm{d}x} = \frac{f_e \varrho}{\varepsilon} j_2. \tag{17}$$

The current density per unit surface area of the electrode material, j_1, is related to the current density per unit area of electrode cross-section parallel to the diaphragm, j_2, by the equation

$$\frac{\mathrm{d}j_2}{\mathrm{d}x} = a j_1. \tag{18}$$

Differentiating Eq. (*17*) with respect to x and using Eqs (*14*) and (*18*), we obtain a differential equation for the potential in a trickle-bed electrode as a function of the distance, x, from the plate current collector:

$$\frac{\mathrm{d}^2E}{\mathrm{d}x^2} = -\frac{2Fa\varrho c_0 f_e \varepsilon^{-1}}{K_0^{-1} + k_1^{-1} \exp\left(\alpha_1 FE/RT\right)}. \tag{19}$$

The initial conditions for the current collector/bed interface are

$$x = 0, \quad \mathrm{d}E/\mathrm{d}x = 0, \quad E = E_0. \tag{19a, b}$$

The first condition arises from the current density in the electrolyte, j_2, being zero at the above interface. The second condition specifies a chosen potential at the current collector for which the current density, current yield and other parameters will be calculated.

The calculation starts by evaluating the mass transfer coefficients and then solving the differential equation (*19*) for a chosen value of E_0 to obtain the dependence of the potential on the coordinate x. The next step is to calculate the current density $j_2(t_e)$ by integration of Eq. (*18*) over the range from 0 to t_e using the generalized trapezoidal rule. The current density $j_2(t_e)$ obtained is used to calculate the peroxide concentration profile in the electrode, the current yield of peroxide, and the losses of peroxide within the electrode.

Calculation of the Peroxide Concentration Profile in the Direction of Electrolyte Flow

The steady-state peroxide concentration in the bed is given by

$$-\nabla J_2 + \delta_2 = 0 \,. \tag{20}$$

In view of the relatively small thickness of the bed and the high turbulences involved, we can neglect the concentration differences in the direction (x) normal to the plane of the plate current collector, and also the concentration gradients along the coordinate z. A mass balance for peroxide over an element of bed width w, bed thickness t_e, and differential height $\mathrm{d}y$ yields

$$-\frac{\mathrm{d}J_2}{\mathrm{d}y} + \bar{\delta}_2 = 0 \,, \tag{20a}$$

where $\bar{\delta}_2$, the mean rate of peroxide formation in the element, is given by

$$\bar{\delta}_2 = \frac{1}{t_e}\int_0^{t_e} \delta_2 \,\mathrm{d}x = \frac{a}{t_e}\int_0^{t_e} r_1 \,\mathrm{d}x - \frac{a}{t_e}\int_0^{t_e} r_2 \,\mathrm{d}x - a r_3 - \frac{N_2}{t_e} \,. \tag{21}$$

The rate of peroxide formation, r_1, is given by Eq. (*14*), and the rate of its reduction, r_2, by the kinetic equation

$$r_2 = k_2 c_2 \exp\left(-\alpha_2 F E / RT\right) \,. \tag{22}$$

According to our measurements[1,2], the decomposition of hydrogen peroxide on the surface of carbonaceous materials is a first-order reaction,

$$r_3 = k_3 c_2 \,. \tag{23}$$

The rate of the transport of perhydroxyl ions across the diaphragm can be approximated by

$$N_2 = D_2 \frac{\varepsilon_d c_2}{f_d t_d} + \frac{c_2 u_2 j_2(t_e)}{F \sum_{i=1}^{3} c_i u_i} . \tag{24}$$

Expressing the flux of perhydroxyl ions through the bed as the sum of the diffusion and convection contributions,

$$J_2 = -D_2 \frac{\varepsilon}{f_e} \frac{dc_2}{dy} + c_2 U_L , \tag{25}$$

and inserting Eqs (*21*) to (*25*) into (*20a*), we obtain a differential equation describing the distribution of peroxide concentration along the bed:

$$D_2 \frac{\varepsilon}{f_e} \frac{d^2 c_2}{dy^2} - U_L \frac{dc_2}{dy} + a c_0 P - a k_2 c_2 Q - a k_3 c_2 -$$

$$- D_2 \frac{\varepsilon_d c_2}{f_d t_d t_e} - \frac{j_2(t_e) c_2 u_2}{F t_e \sum_{i=1}^{3} c_i u_i} = 0 , \tag{26}$$

where

$$P = \frac{1}{t_e} \int_0^{t_e} \frac{dx}{K_0^{-1} + k_1^{-1} \exp(\alpha_1 FE/RT)} \tag{26a}$$

$$Q = \frac{1}{t_e} \int_0^{t_e} \exp(-\alpha_2 FE/RT)\, dx . \tag{26b}$$

The initial conditions for the top of the bed (at the entry of the electrolyte) are

$$y = 0 ; \quad c_2 = 0 , \quad dc_2/dy = 0 . \tag{26c, d}$$

The peroxide concentration profile is obtained by numerical integration of the differential equation (*26*) using the Runge–Kutta–Merson method. The integral rates of the processes occurring in the bed, *i.e.*, the rates of peroxide formation (R_0), reduction (R_1), decomposition (R_2), and transport across the diaphragm (R_3) are given by

$$R_0 = V \frac{a}{t_e} \int_0^{t_e} r_1 \, dx = V a c_0 P \tag{27a}$$

$$R_1 = \int_0^1 \int_0^{t_e} ak_2 wc_2 \exp\left(-\alpha_2 FE/RT\right) \mathrm{d}x\, \mathrm{d}y = ak_2 wt_e Q \int_0^1 c_2 \mathrm{d}y \qquad (27b)$$

$$R_2 = \int_0^1 wt_e ak_3 c_2 \, \mathrm{d}y = wt_e ak_3 \int_0^1 c_2 \, \mathrm{d}y \qquad (27c)$$

$$R_3 = \frac{w\varepsilon_d D_2}{f_d t_d} \int_0^1 c_2 \, \mathrm{d}y + \frac{R_1 + R_2}{R_1} \frac{w}{F} j_2(t_e) \int_0^1 \frac{D_2 c_2}{\sum_{i=1}^{3} D_i c_i} \mathrm{d}y \,. \qquad (27d)$$

The current yield can be calculated from

$$\eta_{H_2O_2} = \frac{R_0 - R_1 - R_2 - R_3}{R_0 + R_1} \,.\, 100 \,. \qquad (28)$$

The integral mean value of the overall current density at the diaphragm is given by

$$j_t = \frac{2F(R_0 + R_1)}{wl} \,. \qquad (29)$$

The relative losses of hydrogen peroxide due to the various processes are given by the ratios

$$Z_i = 100\, R_i/R_0 \,, \quad i = 1, 2, 3 \,. \qquad (30)$$

Accordingly, the calculation of the peroxide concentration profile was made in the following steps:

1. The mass transfer coefficient for oxygen transport from the gas phase to the surface of the electrode material was calculated from Eqs (*1*) to (*11*).

2. Numerical integration of Eq. (*19*) was performed for a chosen initial condition (*19b*) to obtain the dependence of the potential on the *x*-coordinate.

3. The external current density, $j_2(t_e)$, was calculated, and the terms P and Q defined by Eqs (*26a*) and (*26b*) were evaluated.

4. The differential equation (*26*) was integrated numerically to obtain the peroxide concentration profile along the bed length.

5. The current yield of hydrogen peroxide and losses of the peroxide due to its reduction, chemical decomposition and transport across the diaphragm were evaluated.

The calculation was performed on a Hewlett–Packard 9830 desk calculator. The computation of a polarization curve with 20 points lasted 14 min.

Survey and Discussion of Input Data

Electrode: $t_e = 3{\cdot}4 \cdot 10^{-3}$ m, $w = 4{\cdot}5 \cdot 10^{-2}$ m, $l = 0{\cdot}5$ m,

$\bar{d} = 2{\cdot}9 \cdot 10^{-4}$ m (for mesh size 0·18–0·4 mm)
$5{\cdot}2 \cdot 10^{-4}$ m (for mesh size 0·4–0·63 mm)
$8{\cdot}1 \cdot 10^{-4}$ m (for mesh size 0·63–1 mm)

$f_p = 2$, $\varepsilon = 0{\cdot}46$, $f_e = 1{\cdot}4$.

Electrolyte (2M-NaOH): $c_1 = 2\,000$ mol m^{-3}, $h_2 = 1\,080$ kg m^{-3},

$\mu_2 = 1{\cdot}56 \cdot 10^{-3}$ kg m^{-1} s^{-1}, $\varrho = 0{\cdot}04$ Ωm, $D_1 = 5{\cdot}86 \cdot 10^{-10}$ m^2 s^{-1},
$D_2 = 6{\cdot}19 \cdot 10^{-10}$ m^2 s^{-1}, $D_3 = 2{\cdot}86 \cdot 10^{-9}$ m^2 s^{-1}.

Gas (oxygen at 1·1 MPa):

$\mu_1 = 2 \cdot 10^{-5}$ kg m^{-1} s^{-1}, $h_1 = 14{\cdot}6$ kg m^{-3},
$D = 1{\cdot}2 \cdot 10^{-9}$ m^2 s^{-1}, $c_0 = 6{\cdot}05$ mol m^{-3}.

Kinetic data for the reactions:

$k_1 = 4{\cdot}4 \cdot 10^3$ m s^{-1}, $b_1 = \alpha_1 F/RT = 24{\cdot}5$
$k_2 = 5 \cdot 10^{-4}$ m s^{-1}, $b_2 = \alpha_2 F/RT = 12{\cdot}5$
$k_3 = 6{\cdot}5 \cdot 10^{-9}$ m s^{-1}.

Diaphragm:

$t_d = 1{\cdot}5 \cdot 10^{-4}$ m, $\varepsilon_d = 0{\cdot}30$, $f_d = 2{\cdot}63$.

The roughness factor, f_p, for graphite particles was derived from results of our measurements of two-phase pressure drops[12]. The above given value is that for which the best agreement was found between measured and calculated (Eq. (5)) pressure drops. The electrode porosity was calculated from the bulk weight of the material shaken down in the same way as in the preparation of trickle-bed electrodes.

Diffusion coefficient of perhydroxyl ions was taken from the literature[13].

The rate constants of oxygen and peroxide reduction were calculated from results obtained by Tarasevich and Sabirov[14] for a graphite electrode. The values of the constants refer to the equilibrium potential of a hydrogen electrode in the test solution.

The rate constant of hydrogen peroxide decomposition was evaluated from measurements on crushed graphite[12].

The porosity of the diaphragm was determined from its absorptive capacity. The coefficient of pore curvature was calculated from the resistance of the electrolyte in the diaphragm measured by the bridge method and from the diaphragm porosity[12].

RESULTS AND DISCUSSION

The procedure described above was used to calculate the characteristics of trickle-beds composed of various fractions of S42 graphite at an oxygen pressure of 1·1 MPa. The dependences obtained for an electrode of 0·18–0·4 mm particles are shown in Figs 2–7 and those for 0·63–1 mm particles in Figs 6–9.

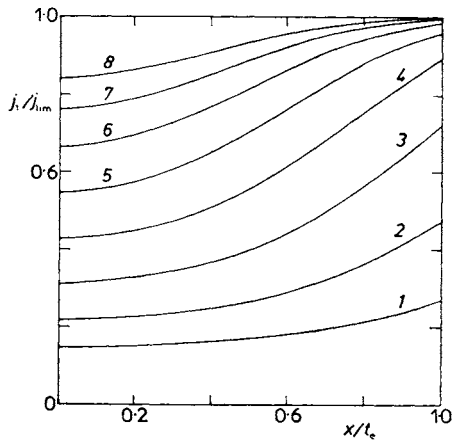

FIG. 2

Calculated dependence of the ratio of local current density for oxygen reduction to limiting current density ($j_{lim} = 2FK_0c_0$) on the relative distance from the current collector at various current densities: *1* 133 A/m^2; *2* 218 A/m^2; *3* 337 A/m^2; *4* 469 A/m^2; *5* 596 A/m^2; *6* 710 A/m^2; *7* 813 A/m^2; *8* 906 A/m^2. Particle size, 0·18–0·4 mm; gas flow rate, 34 dm^3/h; electrolyte flow rate, 0·6 dm^3/h; pressure, 1·1 MPa

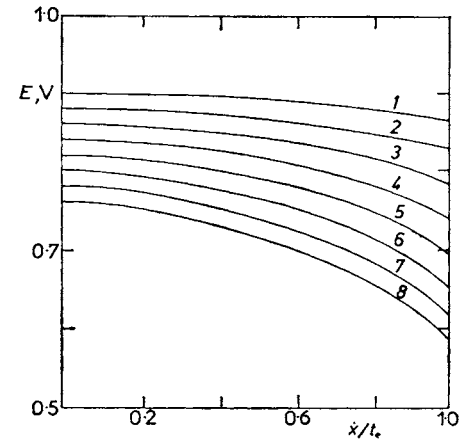

FIG. 3

Calculated dependences of the potential on the relative distance from the current collector. The conditions and notation are the same as in Fig. 2

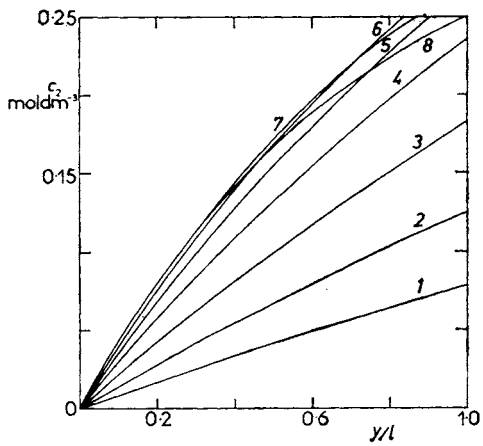

FIG. 4

Calculated dependence of the peroxide concentration in the electrode on the relative distance from the top of the electrode. The conditions and notation are the same as in Fig. 2

The results indicate that the local current density for oxygen reduction increases with the distance from the current collector (Fig. 2). The non-uniformity of the current density distribution is most pronounced at intermediate current densities where the overall process is both oxygen transport and kinetically controlled. At low current densities, the differences are smaller on account of small voltage drops in the electrolyte. The local differences are also small at the highest current densities, where the oxygen reduction is controlled by oxygen transport. According to our calculations in which the solid phase resistance was neglected, the local potential decreases monotonously with the distance from the current collector (Fig. 3).

The dependences of the local current density and the potential on the x-coordinate have also been calculated on the assumption of a limited conductivity of the solid phase in the trickle-bed electrode. These more complicated calculations have shown that the current density is a minimum at the centre of the electrode, increasing towards both the current collector and the diaphragm[12].

An interesting result is the peroxide concentration profile along the electrode length (Fig. 4). While at low current densities the peroxide concentration increases roughly in proportion to the distance from the top of the bed, there is a bend in the $c_2 - y$ curve at higher current densities as a result of more negative potentials and

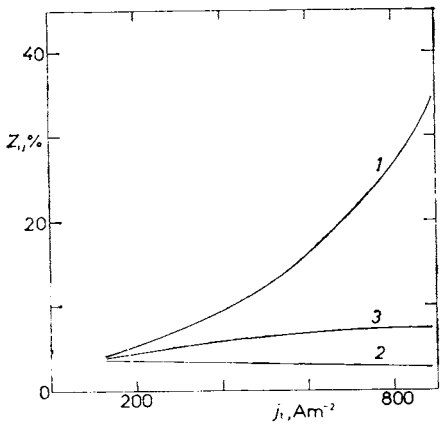

FIG. 5

Calculated dependences of the relative losses of hydrogen peroxide on the overall current density. The conditions are the same as in Fig. 2. *1* rate of peroxide reduction; *2* rate of decomposition; *3* rate of transport into the anode chamber

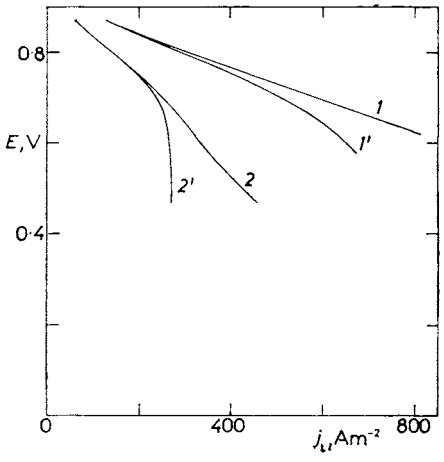

FIG. 6

Calculated partial polarization curves of oxygen reduction (*1'* and *2'*) and total polarization curves (*1* and *2*) of trickle-bed electrodes of 0·18—0·4 mm (curves *1* and *1'*) and 0·63—1 mm particles (curves *2* and *2'*)

hence larger losses of hydrogen peroxide by its reduction. The bend is more pronounced the higher the current density. A practical conclusion is that the optimum current density for the peroxide production depends not only on the kind and size of electrode material particles but also on the electrode length.

The relative losses of hydrogen peroxide in the electrode depend on the current density (Figs 5 and 9). Except at the lowest current densities, the largest loss of hydrogen peroxide is due to its reduction, and this loss increases progressively with increasing current density. The relative loss by decomposition decreases slightly with increasing current density and is found to be several-fold smaller for the coarser fraction. The relative loss of hydrogen peroxide due to its transport across the diaphragm slightly increases with increasing current density. Under conditions where the peroxide concentration decreases with increasing current density (for example, at current densities above 300 A m^{-2}, Fig. 9), a reduction in the peroxide loss by transport is observed.

The rate of perhydroxyl ion transport across the diaphragm has been calculated on the basis of the considerably simplified equation (*24*). However, the applicability

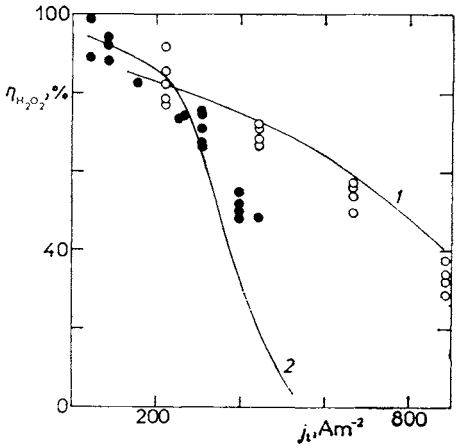

FIG. 7

Calculated and measured dependences of the current yield of hydrogen peroxide on the overall current density for electrodes of 0·18—0·4 mm particles (curve *1*, calculated points; ○, experimental points) and 0·63 to 1 mm particles (curve 2, calculated points; ●, experimental points). The conditions are the same as in Fig. 2

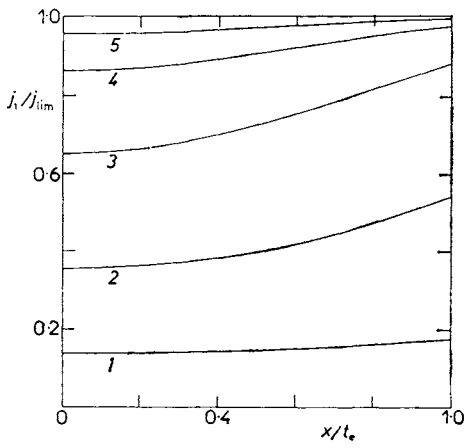

FIG. 8

Calculated dependences of the ratio of local current density for oxygen reduction to limiting current density on the relative distance from the current collector at various current densities: *1* 41 A/m^2; *2* 113 A/m^2; *3* 209 A/m^2; *4* 272 A/m^2; *5* 314 A/m^2. Particle size, 0·63—1 mm; gas flow rate, 34 dm^3/h; electrolyte flow rate, 0·6 dm^3/h; pressure, 1·1 MPa

of this equation under the given conditions has been verified by comparing the results obtained from Eq. (*24*) and by solving a set of non-linear differential equations describing the distributions of the concentrations of all the ions present and the potential in the diaphragm[15] for several model examples. The differences between the results from the two approaches did not exceed 5–20%.

The partial polarization curves for oxygen reduction (Fig. 6, curves *1'* and *2'*) exhibit bends caused by a limited rate of oxygen transport to the particle surface. The overall polarization curves, on the other hand, show a slightly convex shape at low potentials, as a result of increasing oxygen reduction rate with decreasing potential. An increase in the surface area of the electrode particles by a factor of 2·8 causes a 3·4-fold increase in the limiting diffusion current.

No measured polarization curves are shown in Fig. 6 because potential measurements on the beds failed to provide reliable voltage drops across the solid phase, $\varphi_1(0)-\varphi_1(t_e)$. In measuring the voltage between a reference mercuric oxide electrode (with the mouth of the Luggin capillary at the diaphragm), differences $\varphi_1(0)-\varphi_2(t_e)$ were obtained which included the local potential at the diaphragm, $\varphi_1(t_e)-\varphi_2(t_e)$, and the voltage drop across the solid phase of the trickle-bed electrode between the current collector and the diaphragm, $\varphi_1(0)-\varphi_1(t_e)$. The voltage drop was measured with the aid of a nickel gauze inserted between the trickle-bed electrode and the diaphragm. It was found, however, that local potentials calculated on the basis of this quantity decreased in some cases to more negative values with an increase in the electrolyte flow rate or the pressure; in other cases, the calculated local potential at the diaphragm remained constant upon change in the current density. Apparently, the potential of the gauze may not have equalled that of the electrode particles at the diaphragm, for the gauze may have functioned additionally as a cathode, producing an undefinable voltage between itself and the electrode material particles.

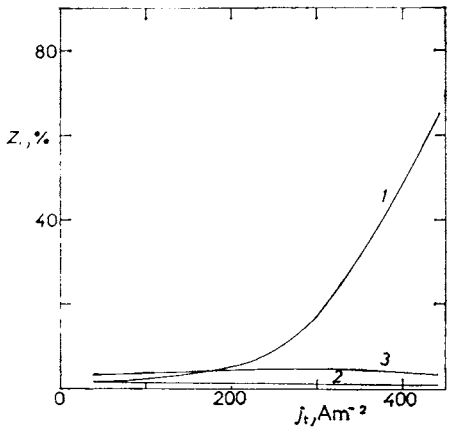

FIG. 9

Calculated dependences of the relative losses of hydrogen peroxide on the overall current density. The conditions are the same as in Fig. 8. For notation, see Fig. 5

A comparison of calculation with experiment can be made on the basis of the variation in the current yield of hydrogen peroxide with the current density. As seen in Fig. 7, the curves calculated for two different trickle-bed electrodes match the measured data quite well. The current yield decreases more rapidly for the electrode of the coarser particles. This is due to a more rapid decrease in the potential and hence a higher rate of peroxide reduction.

The proposed model has been used to calculate the characteristics of the trickle-bed electrode for various input parameters (the gas and electrolyte flow rates, the size of the electrode material particles). There were some differences between the calculated and measured results, the greatest discrepancy being found for the effect of the electrolyte flow rate. According to the calculations, an increase in the electrolyte flow rate should result in an increase in the mass transfer coefficient and hence in a shift of the potential to more positive values. In some of the measurements, however, an increase in the electrolyte flow rate produced the opposite effect. The discrepancy may be explained in that the model identifies the gas/liquid interfacial area with the surface area of the electrode particles, whereas in a real electrode the interfacial area apparently decreases with increasing electrolyte flow rate. This explanation is supported by the observation of high hold-ups of electrolyte at high flow rates (60 to 85% of the void space of the electrode). Under these conditions, a model assuming that the electrolyte flows down over the particle surface in the form of a film apparently does not correspond to the real situation. Actually, the gas fills only some of the intergranular pores or is contained in the gas channels only, so that the gas/liquid interfacial area is considerably lower than the liquid/electrode material interfacial area. This interpretation is in accord with the observation that an electrode composed of very fine particles (0·08 – 0·18 mm) has a higher hold-up than an electrode of coarser particles and also a lower current density than indicated by the model.

The proposed model considering both the kinetics of oxygen reduction and the transport limitations may, on the whole, be evaluated as a first approximation to the performance of a real peroxide-producing trickle-bed electrode. It provides a route for calculating the polarization curves of a trickle-bed electrode and the integral current yields of hydrogen peroxide, and also for evaluating the effects of the various processes on the total loss of hydrogen peroxide. The main flaws of the model are the assumptions of zero resistance of the electrode material and of equal gas/liquid and liquid/electrode material interfacial areas.

The results obtained have shown that the rate of oxygen reduction in a trickle-bed electrode is markedly lower than that in an efficient gas diffusion electrode operated at the same pressure. In a trickle-bed electrode, oxygen passes through a relatively thick layer of electrolyte flowing over the surface of electrode material particles, which imposes a severe transport limitation on the process. For this reason, the potential decreases with increase in the current density more rapidly than it does in

a gas diffusion electrode[16]. The process causing the largest loss of hydrogen peroxide in a trickle-bed electrode is therefore the peroxide reduction, whereas in a gas-diffusion electrode it is the catalytic decomposition[16].

LIST OF SYMBOLS

a	surface area of particles in unit volume of bed, m^{-1}
c_0	oxygen solubility in electrolyte, mol m^{-3}
c_1, c_2, c_3	concentrations of Na^+, HO_2^-, and OH^- ions in electrolyte, respectively, mol m^{-3}
c_s	oxygen concentration at the solid phase surface, mol m^{-3}
d	effective particle diameter, m
d'	modified particle diameter, m
d	arithmetic mean of mesh sizes of a given fraction of electrode material, m
D_1, D_2, D_3	diffusion coefficients of Na^+, HO_2^-, and OH^- ions, respectively, $m^2 s^{-1}$
D	diffusion coefficient of oxygen, $m^2 s^{-1}$
E	local potential in trickle-bed electrode, V
$E(t_c)$	potential at the diaphragm, V
f_e	pore curvature coefficient for the electrode
f_p	roughness factor
f_d	pore curvature coefficient for the diaphragm
g	gravitational constant, 9·81 m s^{-2}
Ga	modified Galileo number
h_G, h_L	density of gas and liquid, respectively, kg m^{-3}
j_1	absolute value of cathodic current density of oxygen reduction per unit area of electrode material, A m^{-2}
j_2	absolute value of current density for oxygen reduction per unit area of electrode cross-section, A m^{-2}
j_{lim}	absolute value of limiting current density per unit area of electrode material, A m^{-2}
j_t	absolute value of total current density at the diaphragm (*i.e.*, for both oxygen and peroxide reduction) per unit external area of diaphragm, A m^{-2}
J_2	flux of perhydroxyl ions along the y-coordinate, mol $m^{-2} s^{-1}$
k_1, k_2, k_3	rate constants of oxygen reduction, peroxide reduction, and peroxide decomposition, respectively, m s^{-1}
K_G, K_L	gas-side and liquid-side mass transfer coefficients, respectively, m s^{-1}
K_S	mass transfer coefficient at the *l–s* interface, m s^{-1}
K_0	overall mass transfer coefficient, m s^{-1}
l	electrode length, m
N	oxygen flux per unit area of electrode material particles, mol $s^{-1} m^{-2}$
N_2	rate of perhydroxyl ion transport across the diaphragm, mol $m^{-2} s^{-1}$
P	defined by Eq. (*26a*)
$\Delta P_G, \Delta P_L$	single-phase pressure drops across electrode, Pa m^{-1}
ΔP_{LG}	two-phase pressure drop, Pa m^{-1}
Q	defined by Eq. (*26b*)
r_1, r_2, r_3	rates of reactions (*A*), (*B*), and (*C*), respectively, mol $s^{-1} m^{-2}$
R_0, R_1, R_2	rates of peroxide formation, reduction, and decomposition, respectively
R_3	rate of peroxide transport across diaphragm, mol s^{-1}
Re_G, Re_L	Reynolds numbers for gas and liquid in electrode, respectively
Sc	Schmidt number ($= \mu/hD$)

t_e	electrode thickness, m
t_d	diaphragm thickness, m
u_1, u_2, u_3	mobility of Na^+, HO_2^-, and OH^- ions, respectively, $m^2\ V^{-1}\ s^{-1}$
U_G, U_L	velocity of gas and liquid in the electrode, respectively, $m\ s^{-1}$
V	total volume of electrode, m^3
w	electrode width, m
x	distance from current collector, m
y	distance from the top of electrode, m
z	length coordinate normal to the xy plane, m
Z_i	relative losses of peroxide, %
α_1, α_2	transfer coefficients for reactions (*A*) and (*B*), respectively
β	electrolyte hold-up in electrode
δ_2	local rate of peroxide formation in unit volume of electrode, $mol\ m^{-3}\ s^{-1}$
ε	electrode porosity
ε_d	diaphragm porosity
ϱ	specific resistance of electrolyte, Ωm
μ_G, μ_L	dynamic viscosity of gas and liquid, respectively, $kg\ m^{-1}\ s^{-1}$
φ_1, φ_2	internal potentials in the solid and liquid phases, respectively, V

REFERENCES

1. Oloman C., Watkinson A. P.: Can. J. Chem. Eng. *54*, 312 (1976).
2. Oloman C.: J. Electrochem. Soc. *126*, 1885 (1979).
3. Oloman C., Watkinson A. P.: Sv. Papperstidn. *83*, 405 (1980).
4. McIntyre J. A., Philips R. F.: *Proc. Symp. Electrochem. Process Plant Des.*, p. 79. Montreal 1982.
5. Davison J. B., Kacsir J. M., Peerce-Landers P. J., Jasinski R.: J. Electrochem. Soc. *130*, 1497 (1983).
6. Levine S., Oloman C.: *Proc. Symp. Electrochem. Process Plant Des.*, p. 98. Montreal 1982.
7. Ergun S.: Chem. Eng. Prog. *48*, 89 (1952).
8. Sato Y., Hirose T., Takahashi I., Toda M.: J. Chem. Eng. Jap. *6*, 147 (1973).
9. Specchia V., Baldi G.: Chem. Eng. Sci. *32*, 515 (1977).
10. Reiss L. R.: Ind. Eng. Chem., Process Des. Develop. *6*, 486 (1967).
11. Satterfield C. N.: AIChE J. *21*, 209 (1975).
12. Špalek O.: unpublished results.
13. Frumkin A., Nekrasov L., Levich B., Ivanov Yu.: J. Electroanal. Chem. *1*, 84 (1959).
14. Tarasevich M. R., Sabirov F. Z.: Elektrokhimiya *5*, 643 (1969).
15. Roušar I., Micka K., Kimla A.: *Technická elektrochemie* 2, p. 202. Academia, Prague 1981.
16. Špalek O.: This Journal *42*, 2747 (1977); *43*, 2499 (1978).

Translated by M. Škubalová.